Damage Detection in Aluminum Plated using the Electro-Mechanical Impedance Technique

Aimy Wissa, McNair Scholar, Penn State University

Faculty Research Adviser: George Lesieutre, PhD
Professor and Department Head Aerospace Engineering Department
College of Engineering
Penn State University

Abstract

The number of aging aeronautical structures has increased significantly in the last few decades with many aircraft being operated well beyond their design lives. The necessity for onboard systems that provide continuous monitoring of a structure's health has become evident. Several methods and techniques can be applied to meet this need. In this paper the electro-mechanical impedance technique was used with piezoelectric transducers to detect the presence of damage in two Aluminum 6061 plates over three different frequency ranges. The effects of the damage location, as well as the damage size on the impedance signal were also investigated. The results showed that electro-mechanical impedance technique was able to detect the presence of the damage through changes in the real impedance against the frequency over the different frequency ranges. Furthermore, a damage index calculation was carried out to examine the effect of the damage location and size. The results indicated that the bigger the damage size the higher damage index, and that far-field damage results in a smaller damage index than near-field damage.

1. Introduction

1.1 Motivation for Structural Health Monitoring (SHM)

The number of aging aeronautical structures has increased significantly in the last few decades. A large number of aircraft have been performing beyond their design lives. The data in Table 1.1 show that the number of aging aircraft is significant. The number of civil aircraft that have been in service for more than 15 years has increased from 4600 in 1997 to 4730 in 1999. Also, the number of aircraft that have been in service for more than 25 years has increased from 1900 in 1997 to 2130 in 1999. Not only civil aircraft, but also military aircraft have been suffering from the same problem in a more serious fashion. Table 1.2 shows that an increasing number of military aircraft have been in service for more than 40 years [Staszewski 2002]. A study made by Penney indicated that in 2000, over 75% of the US Air Force aircraft were more than 25 years old [Penney 2000].

The problem with aging aircraft is that the longer the aircraft is in service the more operational loads and fatigue it experiences. This means that the older the aircraft the more damage it may suffer. More importantly, due to their long operational life, aging aircraft require higher levels of maintenance and more frequent inspections [Staszewski 2004].

Table 1.1: Aging Civil Aircraft Overview [Staszewski 2002]

Aircraft type	Total delivered	Fleet in service 09/01	Ageing aircraft in 1999		
			≥15 Years	≥20 Years	≥25 Years
A300	503	411 (82 %)	220 (46 %)	60 (12 %)	1 (0,2 %)
A310	255	218 (85 %)	54 (21 %)	–	–
707/720	1009	379 (37 %)	–	–	–
727	1831	1247 (68 %)	1381 (75 %)	1127 (62 %)	673 (38 %)
737–100/200	1144	901 (79 %)	853 (75 %)	442 (39 %)	222 (19 %)
737 CFMI	1988	1971 (99 %)	13 (0,7 %)	–	–
747–100/SP/ 200/300	724	562 (78 %)	490 (68 %)	317 (44 %)	154 (21 %)
757	968	943 (97 %)	51 (6 %)	–	–
767	840	820 (98 %)	109 (14 %)	–	–
DC-8	556	243 (44 %)	268 (48 %)	268 (48 %)	268 (48 %)
DC-9	976	727 (74 %)	776 (79 %)	739 (75 %)	588 (61 %)
DC-10	446	397 (89 %)	333 (75 %)	276 (62 %)	162 (36 %)
L-1011	249	155 (62 %)	185 (74 %)	113 (45 %)	60 (24 %)
Total	11489	8974	4733 (46 %)	3342 (33 %)	2128 (21 %)

Table 1.2: Aging Military Aircraft Overview [Staszewski 2002]

Aircraft Type	First built	Total in service 09/2001	Life extension until
BAE Hawk/Boeing T-45 Goshawk	1976	641	
Boeing F/A-18 Hornet/Super Hornet	1978	1762	2019
Boeing B-52H Stratofortress	mid 50ies	94	2045
Boeing 707/C-137/C-18/KE-3	60ies	97	2030
McDonnel Douglas F-4 Phantom	1958	889	
Dassault/Dornier Alpha Jet	1973	289	
Lockheed-Martin F-16	1974	3398	
Northrop T-38	1959	685	2040
Panavia Tornado	1974	746	2018
MiG-21 (incl. licences)	mid 50ies	3324	
L-39/L-39 Albatros/L-159	mid 70ies	2233	

The maintenance of complex structures like aircraft is very detailed and complicated. It also involves a lot of money and effort. Both civil and military aircraft are currently inspected using visual inspections, as well as on-ground non-destructive testing (NDT). During visual inspections, the human eye or cameras, perhaps aided by dye penetrant are used to detect surface damages. There are several methods for NDT. The most common techniques used are ultrasonic inspection, eddy current and acoustic emission.

The ability to regularly inspect aircraft and predict damage growth reduced the life-cycle cost of aircraft by changing the aircraft design methodology from “safe life” to “fail safe”. In the safe life design method, aircraft structural components are guaranteed to perform safely for a predetermined period of time and then retired at the end of the that period, while in the fail safe design method critical structures in the aircraft are inspected periodically to ensure the safety of

the aircraft structure in between inspections. On the other hand, NDT is still a costly method of inspection due to the short inspection intervals and the intensive labor. The average cost for this approach to damage monitoring is 10.5 billion dollars per year and typical civil aircraft, like the Boeing 747, are inspected every 12 to 17 months [Staszewski 2004]. The high cost of maintenance and labor, as well as the down time that the inspected aircraft experience motivate the development of new methods for monitoring the health of aircraft structures.

A method that has been under development since the early 1990's is an onboard structural health monitoring (SHM) system. In principle a SHM system would be an integrated part of a structure. SHM will potentially reduce the cost of maintenance and inspection. It will also decrease human errors, as well as the labor cost associated with the scheduled inspections. The SHM system may reduce the down time associated with inspections and therefore increase the profit for both the aircraft manufacturers and airlines. SHM will provide continuous interrogations of the structure and therefore increase the reliability and safety of the aircraft by preventing catastrophic structural failures.

1.2 Structural Health Monitoring System Components

SHM systems contain three essential components. The first component involves the sensors and/or sensor networks. Different types of sensors are available for use in a structural health monitoring system. These sensors include piezoelectric, fiber-optic, micro-electromechanical systems and strain gages. The second component of a SHM system is the integrated hardware, which performs the signal conditioning tasks. These tasks include amplifying the signals emitted by the sensors and digitizing them so that they are ready for processing. Finally, the third component is the software that is used to analyze and process the data [Beard 2005].

All of the sensors listed above have been tested and proved to have useful applications in the field of health monitoring. However, piezoelectric transducers are known for their ease of integration within the aircraft structures without interfering with its mechanical systems. Another great advantage of piezoelectric transducers is that they can act as both transmitters and receivers of mechanical signals [Giurgiutiu 2002]. This unique characteristic of the transducers allow them to be used actively, passively or both actively and passively in the same system.

1.3 Structural Health Monitoring System Technologies

Piezoelectric transducers can be used passively in the acoustic emission (AE) technique of health monitoring. In this technique the piezoelectric transducers are used as receivers only. The AE phenomena is based on the release of energy in the form of an elastic wave, also called a stress wave, which is produced by the creation of damage or a defect in the structure. These waves are then detected by the piezoelectric sensors mounted on the structure's surface, where they get converted to voltage signals [Finlayson 2000] and [Balageas 2006]. This technique is well known for its maturity and proven damage detection ability. However, the real challenge in applying this technique is the background noise due to airflow, vibration and electromagnetic interference [Balageas 2006].

Piezoelectric transducers can also be used actively through the acousto-ultrasonic technique (AU). In this technique, piezoelectric transducers are used as both transmitters and receivers. The transducers produce and receive high frequency waves. These waves propagate through the structure and are received once again by the sensors to be analyzed for changes and defects in the structure. This technique is very effective in detecting damage in the form of geometric discontinuities. In addition, this method of health monitoring is able to collect a lot of information about the structure. This technique is costly because it requires a lot of hardware and software to transmit and process a huge amount of data [Balageas 2006].

Finally, piezoelectric transducers can be used in the electro-mechanical (E/M) impedance technique of health monitoring. The E/M impedance technique is a mixed technique, which means that it uses piezoelectric transducers both actively and passively. In this technique the damage in a structure is detected by monitoring the electro-mechanical impedance of the piezoelectric transducers bonded to the structure over a large range of frequencies. The frequency response of the electric impedance reveals changes in the state of the structure's health [Giurgiutiu 1998]. This technique is very effective at ultrasonic frequencies where local damage can be detected more accurately. Also it can give accurate results because the high-frequency response is hardly affected by the global (far-field) conditions of the structure. On the other hand, this technique is best suited to detecting local (near-field) structural defects and therefore it cannot be used to detect far-field damage [Zagrai 2002].

In this paper the electro-mechanical impedance technique was used with piezoelectric transducers to detect the presence of damage in two Aluminum 6061 plates. The effects of the damage presence and location on the impedance signal were investigated. Also the size of the damage was studied and the relationship between the damage size and the produced impedance signal was evaluated.

2. Theory

Piezoelectricity is an electric polarization effect due to mechanical forces. Piezoelectricity was first discovered by Jacques and Pierre Curie in 1880 and it is a property of some crystalline materials. Piezoelectric materials include both natural and artificial materials. Natural materials include quartz (SiO_2), Rochelle salt and tourmaline. Artificial materials include piezoelectric ceramics, piezoelectric polymer films and other materials. The most commonly used piezoelectric materials are lead zirconate titanate (PZT) which is a ceramic, and polyvinylidence fluoride (PVDF) which is a polymer [Staszweski 2004].

Most piezoelectric materials exhibit coupled electric and mechanical properties. Equation 1 describes the linear mechanical behavior of materials. Similarly, Equation 2 describes the electrical properties of dielectric materials.

$$\{T\} = [c^E]\{S\} \quad (1)$$

$$\{D\} = [\varepsilon]\{E\} \quad (2)$$

where S is mechanical strain, T is the mechanical stress in newtons per square meter (N/m^2), D is the charge displacement in coulombs per square meter (C/m^2), E is the electric field in volts per meter (V/m), c is the elastic stiffness of the material in newtons per square meter (N/m^2), and ε is the permittivity in farads per meter (F/m) [Staszweski 2004].

Piezoelectric materials couple mechanical and electrical properties. As shown in Figure 1, the direct piezoelectric effect is where an electric charge is caused by a mechanical stress, and the converse piezoelectric effect is where a strain is produced due to an applied electric field1). Equations 3 and 4 describe the converse and direct effects of piezoelectric materials, respectively.

$$[c^E]\{S\} - [e]\{E\} = \{T\} \quad (3)$$

$$[e]\{S\} + [\varepsilon^S]\{E\} = \{D\} \quad (4)$$

Where e is the piezoelectric coefficient and the superscript t indicates transpose. Additionally the superscripts S and E indicate that the quantities are defined at constant strain and electric field, respectively.

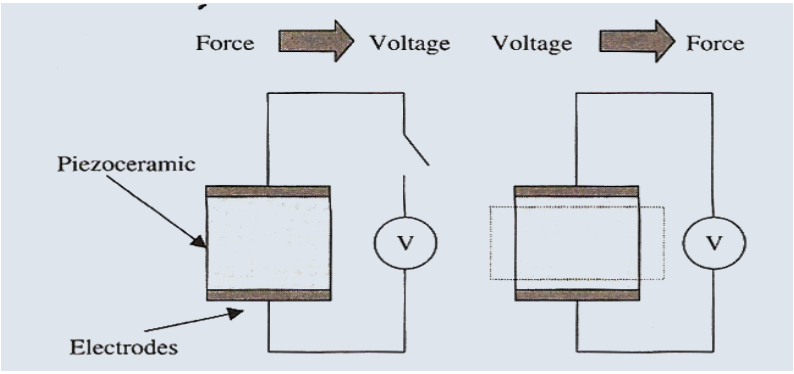

Figure 1: Direct and Inverse effects of Piezoelectric Materials [Staszewski 2004]

As mentioned in the preceding discussion, the electro-mechanical impedance technique uses both the direct and converse effects of piezoelectric materials. The behavior of structures with piezoelectric elements can be modeled using Equations 5 and 6.

Equations of Motion:

$$[M]\{\ddot{x}\} + [K^E]\{x\} - [p]^t\{V\} = \{f(t)\} \quad (5)$$

Charge Equation:

$$[p]\{x\} + [C^S]\{V\} = \{Q\} \quad (6)$$

where M is the mass, K is the stiffness of the structure, p is the coupling term, V is the voltage, f is the external force, C is the capacitance, Q is the charge and x is the displacement.

Assuming that f is equal to zero, then taking the first derivative of Equation 6 with respect to time and taking the Laplace transform of Equations 5 & 6, the resulting equations, neglecting the initial conditions, are

$$\{X\} = \frac{[p]^t}{(s^2[M] + [K^E])}\{\Delta\} \quad (7)$$

$$s[p]\{X\} + s[C^S]\{\Delta\} = \{\varphi\} \quad (8)$$

where X, Δ, φ are the Laplace transforms for the displacement, voltage and current, respectively. Substituting Equation 7 into Equation 8 and collecting similar terms results in

$$\left(\frac{s[p][p]^t}{s^2[M] + [K^E]} + s[C^S]\right)\{\Delta\} = \{\varphi\} \quad (9)$$

Electrical impedance is defined as the ratio of the voltage to the current; hence the impedance can be written as

$$\{Z\} = \frac{\{\Delta\}}{\{\varphi\}} = \frac{1}{\left(\frac{s[p][p]^t}{s^2[M] + [K^E]} + s[C^S]\right)} \quad (10)$$

Converting the electrical impedance equation, Equation 10, from the Laplace domain to the frequency domain by evaluating it at s = iω, the final impedance equation is

$$\{Z\} = \frac{1}{\left(\frac{(i\omega)[p][p]^t}{(i\omega)^2[M] + [K^E]} + (i\omega)[C^S]\right)} \quad (11)$$

From Equation 11 it is clear that the electric impedance depends on the mechanical stiffness of the material [K]. Since the stiffness of a structure is affected by damage, electrical impedance measurements can in principle be used to detect damage in the structure. This is the basic idea behind the "electro-mechanical impedance" method used in this research.

3. Experimental Procedure

The experimental procedure for this experiment can be divided into three main sections. The first section involves preparing the transducers for the experiment, the second is mounting the transducers on the structure, and the third is carrying out the experiment to measure the electrical impedance.

3.1 Preparing the Transducers for the Experiment

Two 1.01 mm (0.0397 inches) thick piezoelectric ceramics, manufactured by APC, were used during this experiment. The ceramics were cut to the desired length and width, 12.7 mm x 12.7 mm (0.5"X0.5"), as shown in Figure 2.

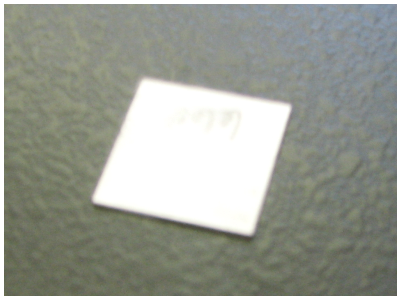

Figure 2: Piezoelectric Transducer

3.2 Experimental Setup

Two mirror-finished Aluminum 6061 plates were used in this experiment. The thickness of each plate was 1.575 mm (0.062 inches) and the dimensions were 30.48 cm x 30.48 cm (12"x12"). Both the negative side of the transducers and the plates were lightly sanded and cleaned to give better adhesion. Epoxy was used to attach each transducer to the center of its corresponding plate, as shown in Figure 3. After ensuring that the piezoelectric transducers were well-adhered to the surface of the aluminum structure and after running several conductance tests, wires were soldered to the transducers.

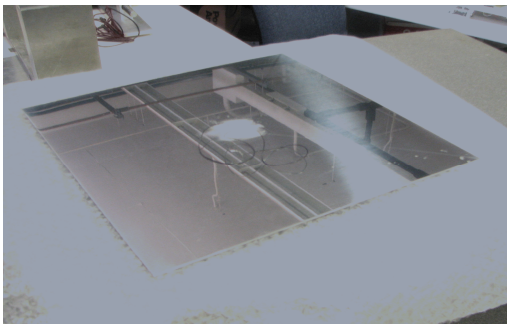

Figure 3: Transducer mounted on the corresponding Plate

3.3 Experimental Procedures

Several frequency bands were used during this experiment. These bands were 10-500 kHz, 50-80 kHz and 380-480 kHz. The plates were placed on foam to simulate the free-free boundary conditions. Electrical impedance measurements were collected using an Agilent 4294A precision impedance analyzer, shown in Figure 4. The electric impedance, both magnitude and phase, were measured over all frequency ranges for the undamaged plates. The data were compared to ensure that both plates were similar. Figures 5a and 5b show the similarity between the impedance signals for the undamaged plates.

Figure 4: Agilent 4294A Impedance Analyzer

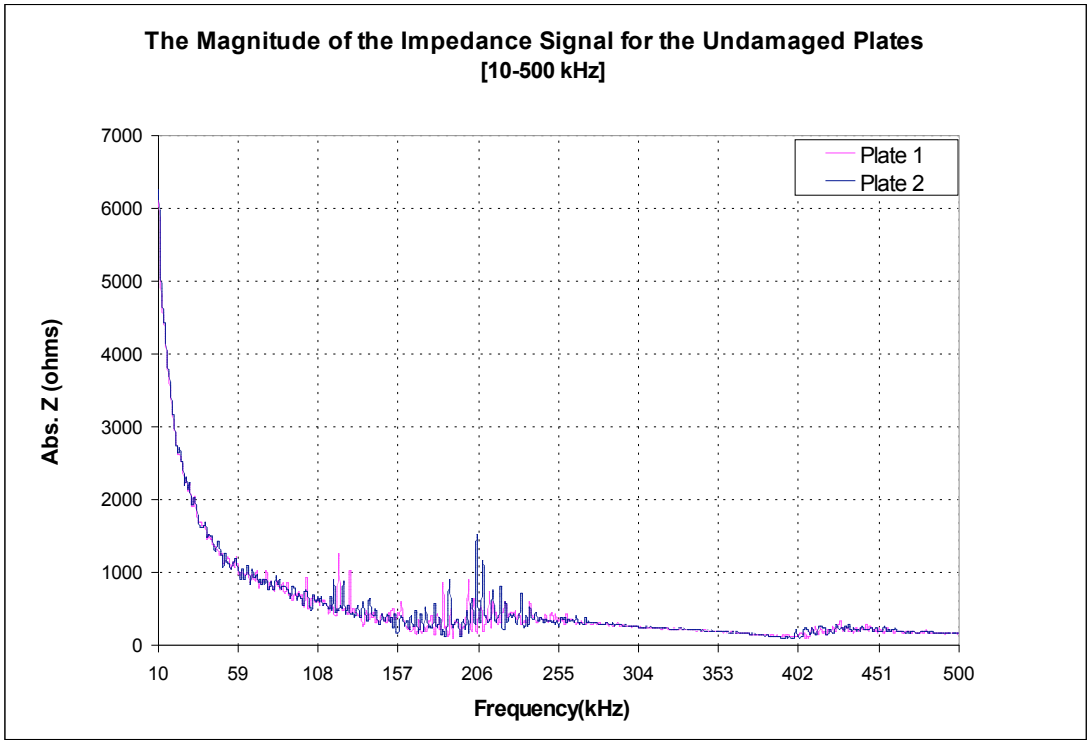

Figure 5a: The magnitude of Electric Impedance Signal for the Undamaged Plates

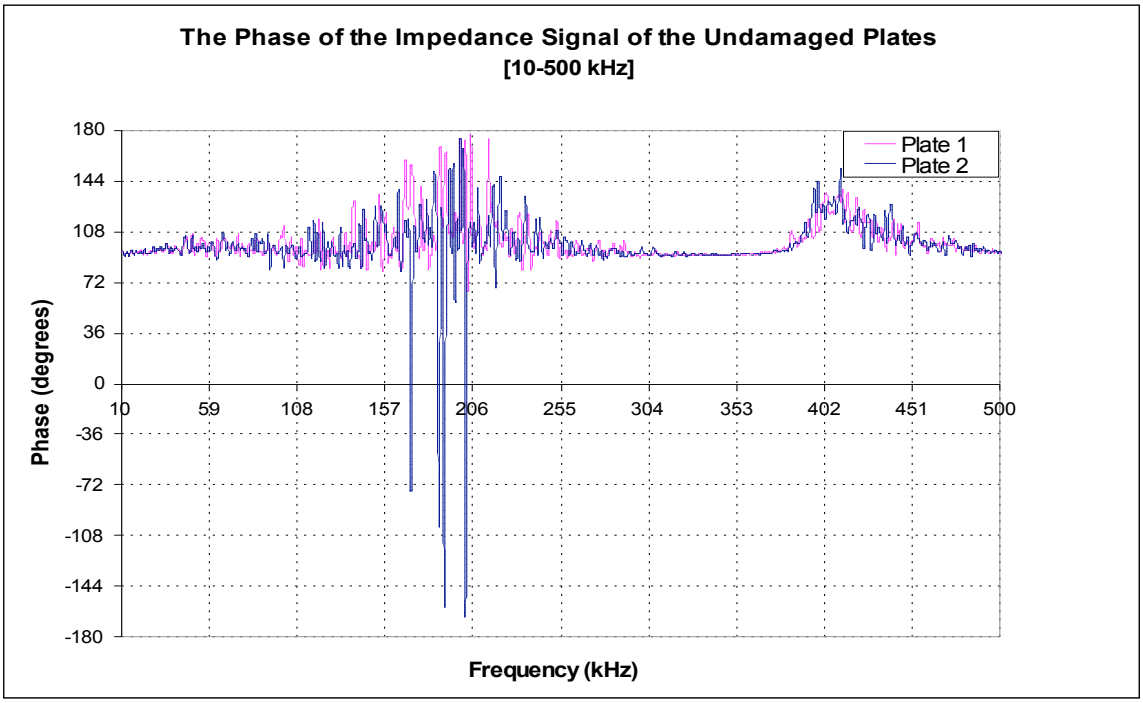

Figure 5b: The Phase of Electric Impedance Signal for the Undamaged Plates

A Dremel was then used to introduce a 15 mm slit 15 mm away from the end of the transducer on the first plate and the same size slit was introduced 5 mm away from the end of the transducer on the second plate as shown in Figure 6. The electric impedance, both magnitude and phase, of each plate was recorded again and compared against that of the other plate, as well as that of the corresponding undamaged plate. The slit sizes were then increased in increments of 5 mm until they reached a width of 40 mm as shown in Figure 7.

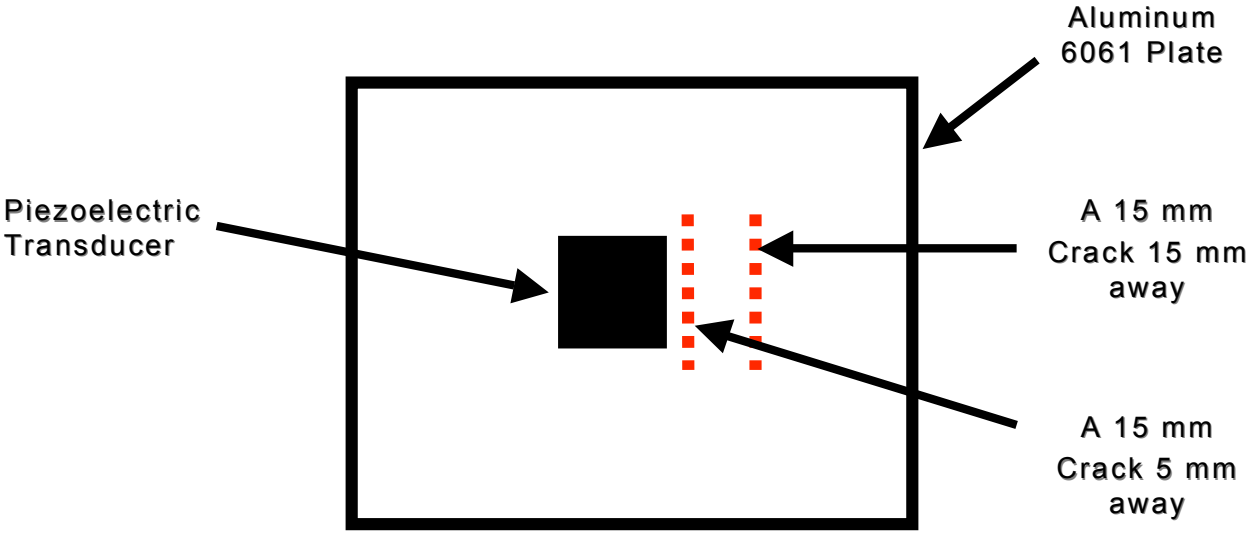

Figure 6: A schematic diagram of the Slit location

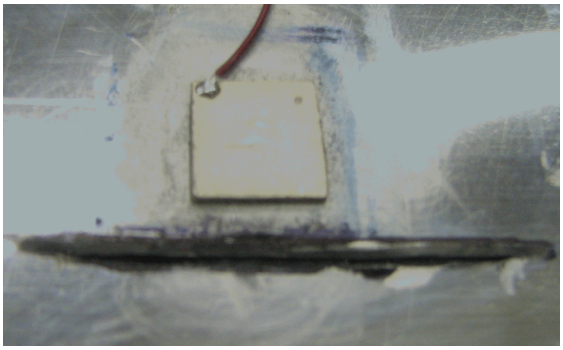

Figure 7: 40 mm slit introduced in the Plate using the Dremel

After collecting the impedance and phase data for all the damage sizes and locations, the impedance was expressed in terms of real and imaginary parts. The real part was plotted against the frequency to detect the effect of the damage presence, as well as its location and size [Giurgiutiu 2002].

A damage index calculation was carried out using the real part of the electric admittance [Y] of the damaged and undamaged structures. Electric admittance is defined as the ratio of the resulting current to the energizing voltage, or the inverse of the impedance. The damage index metric (M) used in this experiment is expressed in Equation 12 [Chaudhry 1995] and it was used

to investigate the relationships and the correlations between the damage size and location and the impedance signal.

$$M = \sum_{i=1}^{N} [\mathrm{Re}(Y)_{undamaged} - \mathrm{Re}(Y)_{Damaged}]^2 \qquad (12)$$

4. Results and Discussion

The results of this experiment can be divided into several parts. The first part addresses the general effects of the damage presence on the real part of the impedance signal. The second part addresses the effect of the damage location on the real part of the impedance signal, and the third part addresses the effect of the damage size on the real part of the impedance signal.

4.1 The General Effects of the damage Presence on the real part of the impedance signal

The presence of damage affected the impedance signal at all frequency ranges as shown in Figures 8 through 10. Figure 8 shows a general shift in the frequency of the impedance peaks to lower frequencies over a wide range of frequencies, 10-500 kHz.

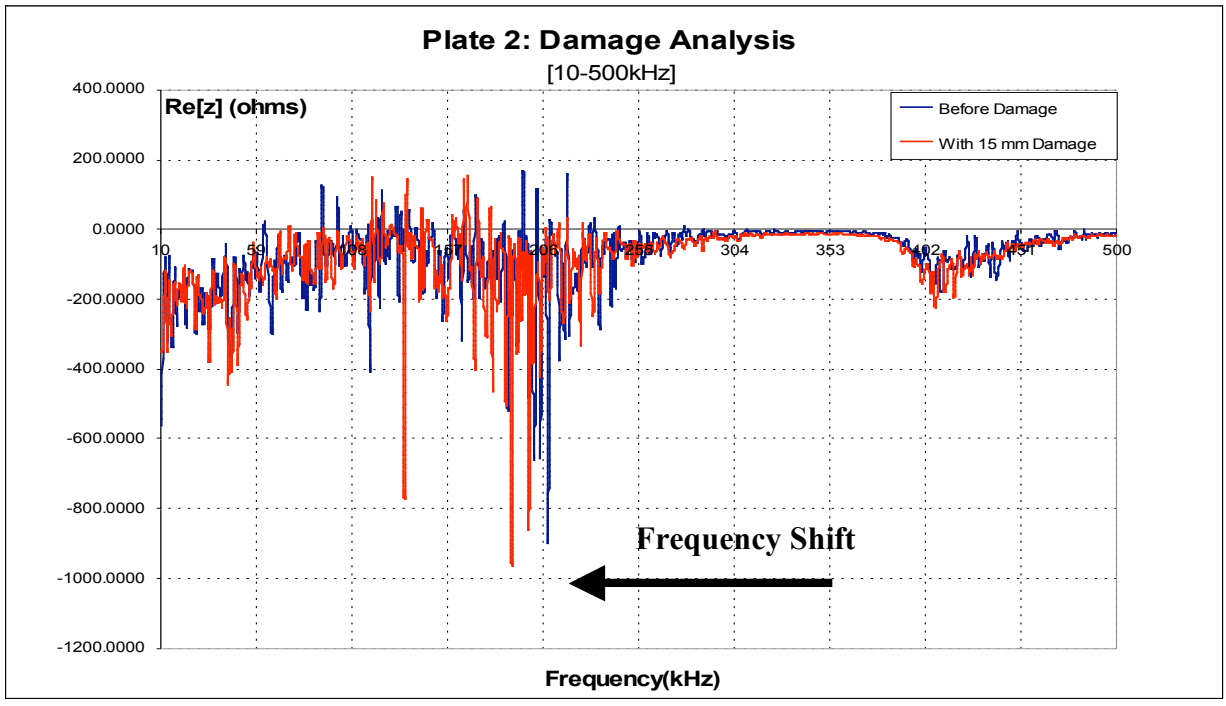

Figure 8: Damage Presence Analysis at 10-500 kHz

Also in Figure 9, which shows the behavior of the real part of the impedance signal in the 50 kHz to 80 kHz frequency, one sees a considerable decrease in the amplitude of peaks in the real part of the impedance.

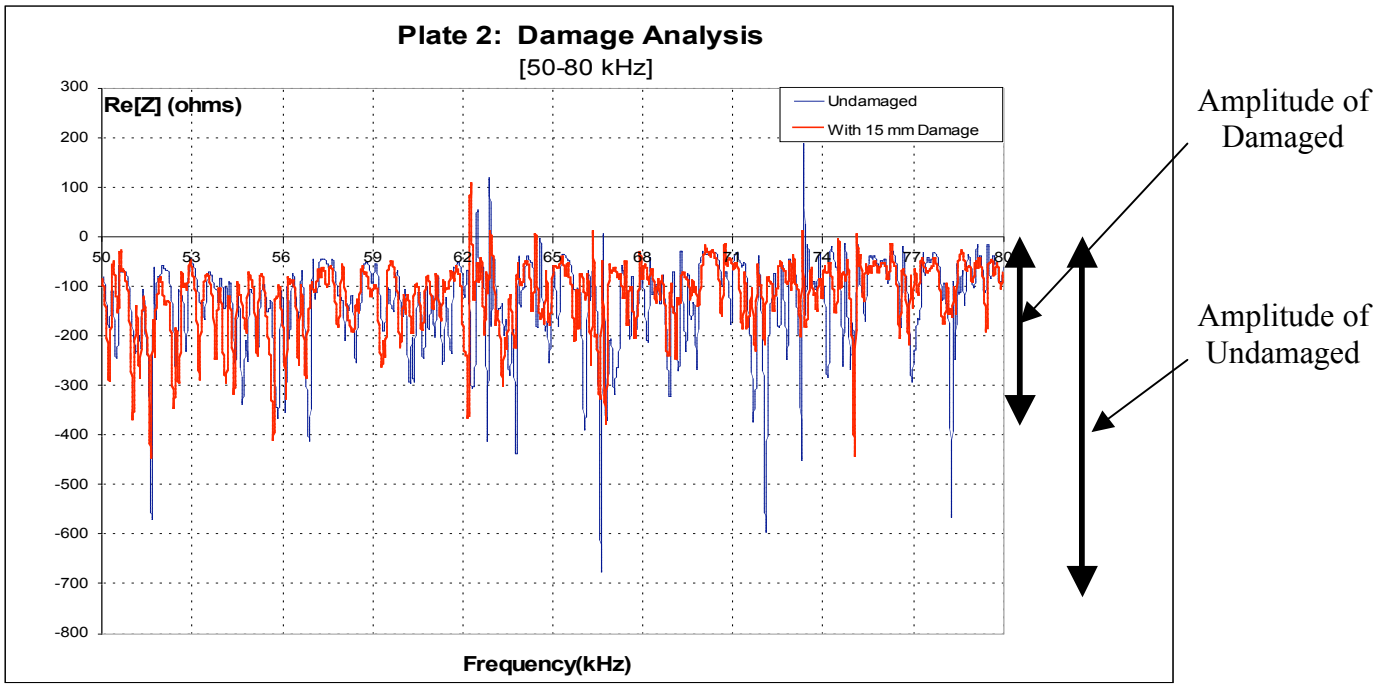

Figure 9: Damage Presence Analysis at 50-80 kHz

Meanwhile, Figure 10 that describes the behavior of the real part of the impedance signal at the higher frequency band, 380-480 kHz, shows both a downward shift in the frequencies of the impedance peaks and a decrease in the amplitude of the peaks. At this frequency range, the impedance peaks tend to occur at lower frequencies and with lower amplitudes.

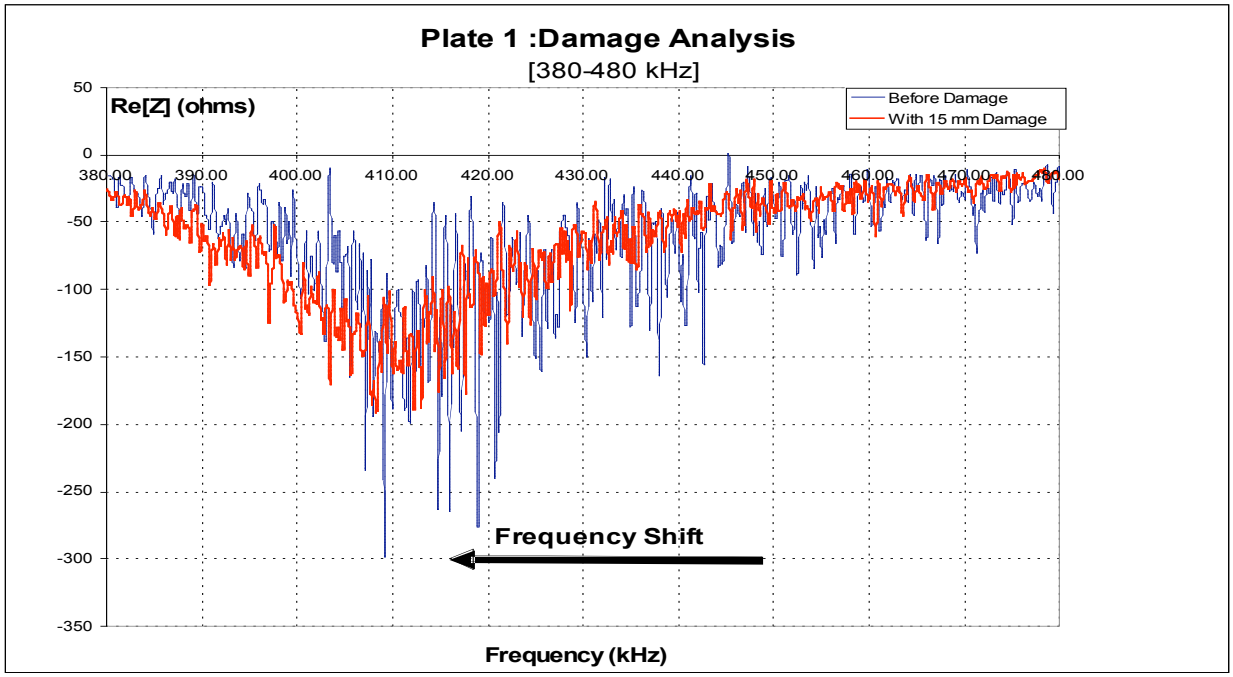

Figure 10: Damage Presence Analysis at 380-480 kHz

4.2 The Effect of Damage Size on the Impedance Signal

The damage size was increased from 15mm to 40 mm in increments of 5mm. As the damage size increased, the effects mentioned for the presence of damage became more. Figure 11 shows that increasing the damage size to 40 mm, at the higher frequency range, led to a greater decrease in the amplitude of the frequency peaks and a larger frequency shift in the impedance peaks.

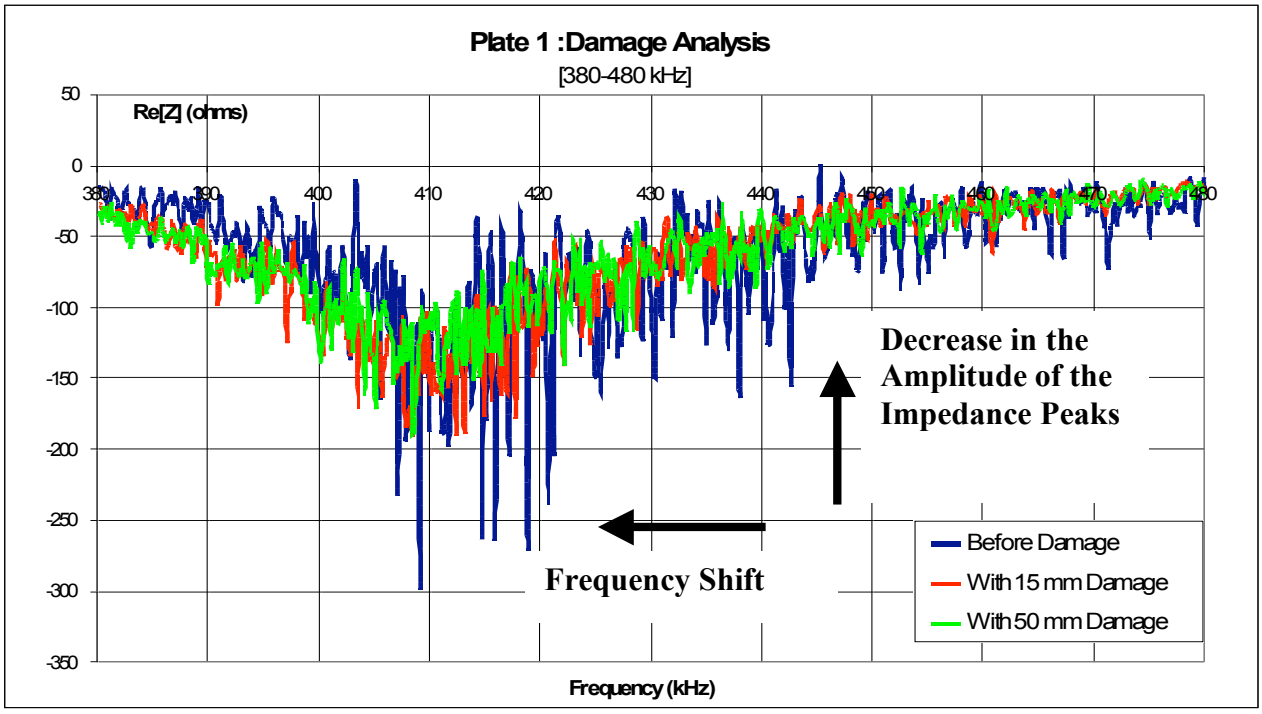

Figure 11: The Effect of increasing the Damage Size on the Impedance Signal at 380-480 kHz

After plotting the real part of the impedance against frequency over the different frequency ranges, Equation 12 was used to calculate the damage index for each damage size. Figure 12 indicates that as the damage size increased the damage metric increased and the increase was almost logarithmic with the size, as shown in Equation 13.

$$y = 1E-06\ln(x) + 4E-06 \qquad (13)$$

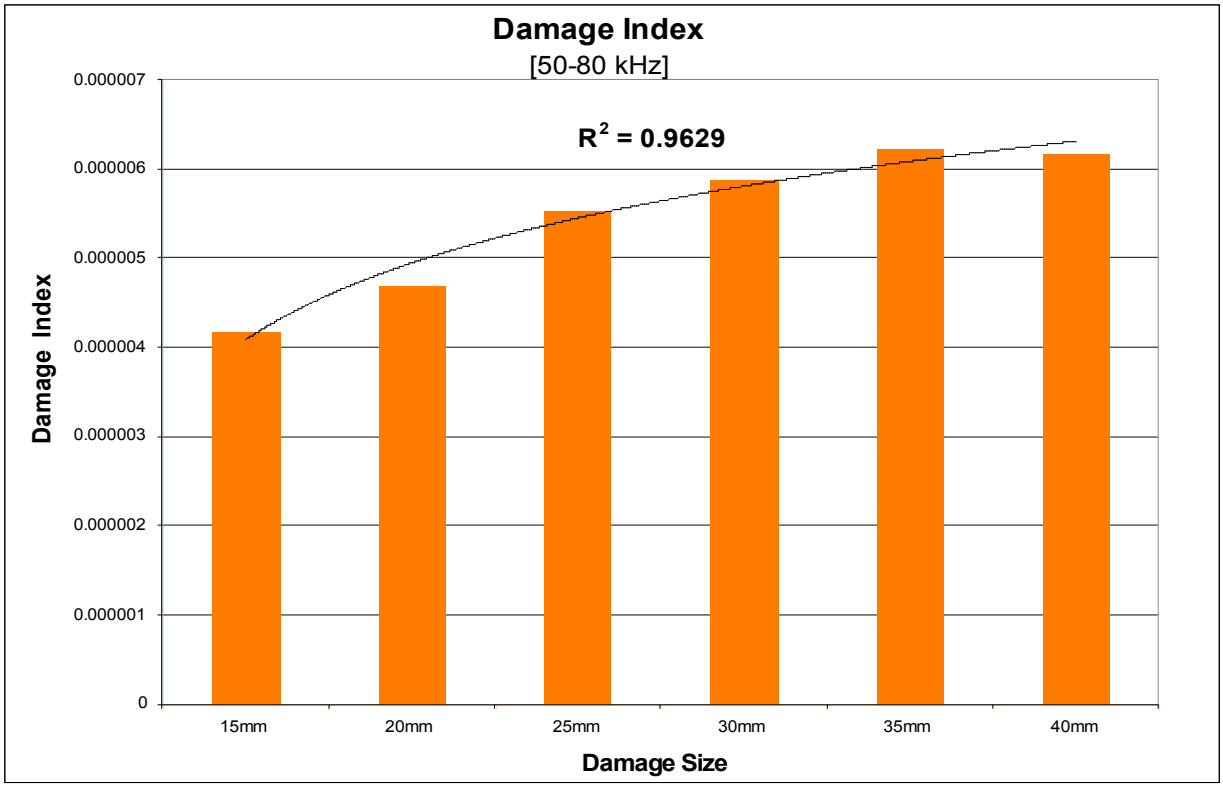

Figure 12: The Damage Index Metric for detecting the Effect of the Damage Size at 50-80 kHz

4.3 The Effect of the Damage Location on the Impedance Signal

Other literature mentioned that the electro-mechanical impedance method is better at detecting local or near-field damage [Giurgiutiu 2002, Balageas 2006]. In the present experiment, as the damage distance increased the damage index decreased for every damage size. Figure 13 shows the effect of the damage location on the damage index at the various damage sizes. This indicates that global or far-field damage is less likely to be detected using the electromechanical impedance method. Also, from the same figure, Figure 13, the increase in the damage index of the far field damage is less accurate than that of the near-field. This can also be related to the fact that far field damage is not as accurately determined by this method.

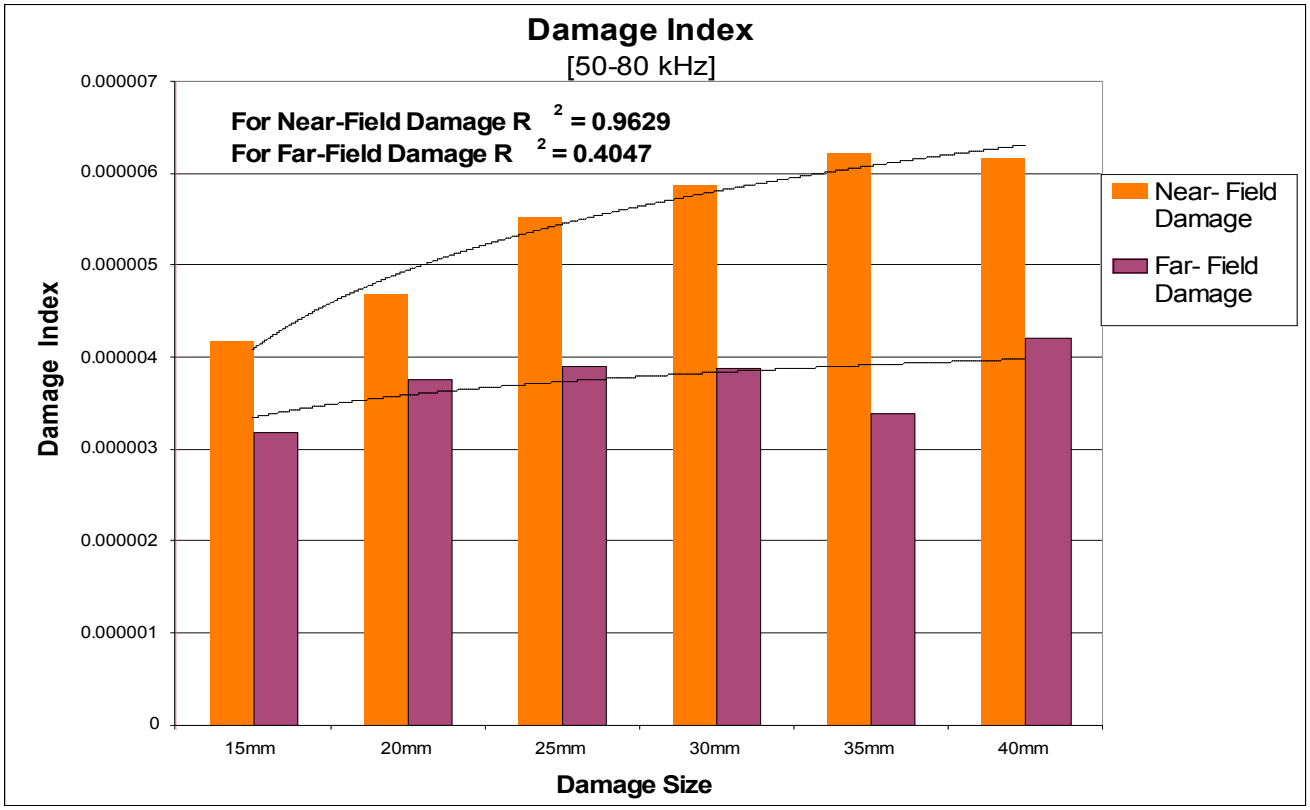

Figure 13: Near Field and Far Field Damage Index

5. Conclusion

In this paper the electro-mechanical impedance method was used to detect damage in two aluminum 6061 plates. The method used piezoelectric transducers both actively and passively. The electro-mechanical impedance method using the piezoelectric transducers proved its ability in detecting the presence of damage, as well as its location and size.

The effect of the damage presence was evident in the reduction of the magnitude of peaks in the real part of the impedance, as well as the frequency shift of the peaks. The effect of increasing the damage size was detected through a damage index calculation. The results indicated that increased damage increased the damage index. Furthermore, the electro-mechanical impedance method was more accurate in detecting near-field (local) damage than it was detecting far-field (global) damage. The difference in the damage location was observed through the same damage index calculations showed that distant damages produced smaller damage indices than these located closer to the transducers.

6. Recommendations and Future Work

Although the E/M impedance method was effective in detecting both near- field and far-field damage, with different degrees of accuracy, further efforts are needed to determine the distance at which the transducer can no longer detect damage using this method. Also a detailed study of the best location for the transducer at the different boundary conditions is needed. Finally, in order to integrate the electro-mechanical impedance method in the aerospace industry, further efforts are needed to decrease the amount of wiring involved in this method and the size of the hardware used.

7. Acknowledgments

The author would like to thank the McNair Scholars Program at the Pennsylvania State University for funding this research program. In addition, the help and supervision of Dr. George Lesieutre, Professor and head of the Aerospace Department at the Pennsylvania State University, is acknowledged thankfully. Finally, all the help and advice provided by Mr. Michael Theil is greatly appreciated.

8. References

1. Balgageas, D., Fritzen, C. and Güemes, A. 2006. Structural Health Monitoring, *Wiltshire, Great Britain.*
2. Beard, S., Kumar, A., Qing, X., Chan, H., Zhang, C., and Ooi, T. 2005. Practical Issues in Real World Implementation of Structural Health Monitoring Systems, *Proceedings of SPIE on Smart Structures and Material Systems*, March
3. Chaudhry, Z., Joseph, T., Sun, F. and Rogers, C. 1995. Local-area Health Monitoring of Aircraft via Piezoelectric Actuator/Sensor Patches, *Proceedings of SPIE*, Vol. 2443, (pp.268-276)
4. Finlayson, R., Friesel, M., Carlos, M., Cole, P. and Lenain, J. 2000. Health Monitoring of Aerospace Structures with Acoustic Emission and Acousto-Ultrasonics, *Proceedings of the 15th World Conference on Non-Destructive Testing*, *Roma, Italy*, 15-20 October
5. Giurgiutiu, V. and Rogers, C. 1998. Recent Advancement Electro-Mechanical (E/M) Impedance Method for Structural Health Monitoring and NDE, *Proceeding of the SPIE 5th Annual International Symposium on Smart Structures and Materials, California, U.S.A*, 1-5 March, Paper# 3329-53.
6. Giurgiutiu, V., Zagari, A. and Bao, J. 2002. Piezoelectric Wafer Embedded Active Sensors for Aging Aircraft Structural Health Monitoring, *Structural Health Monitoring*, Vol.1 (pp.41-60)
7. Penny,S. 2000. Geriatric ward, *Flight International*, 12-18 December.
8. Staszewski, W.J. and Boller, C. 2002. Acoustic Wave Propagation Phenomena Modeling and Damage Mechanisms in Ageing Aircraft, *Aircraft Integrated Monitoring System (AIMS)*, *Garmisch-Partenkirken, Germany,* 27-30 May*,* CD-ROM *Conference Proceedings,* (pp.169-184)
9. Staszweski, J., Boller, C. and Tomlinson. G. 2004. Health Monitoring of Aerospace Structures: Smart Sensor Technologies and Signal Processing, *Munich, Germany*
10. Zagari, A. and Giurgiutiu, V. 2002. Health Monitoring of Aging Aerospace Structures using The Electro-Mechanical Impedance Method, *Proceedings of SPIE*, Vol. 4702, (pp.289-300)